energy&fuels

pubs.acs.org/EF

Article

# Molecular Dynamics Study on the Capture of Aluminum Particles by Carbon Fibers during the Propagation of Aluminum-Based Energetics

Yuxin Zhou and Michael R. Zachariah*

Cite This: *Energy Fuels* 2024, 38, 8992−9000

Read Online

ACCESS | Metrics & More | Article Recommendations | Supporting Information

**ABSTRACT:** Previous experimental results have shown that carbon fibers (CF) can significantly promote the propagation of aluminum-based nanothermites and propellants. To explore the mechanism of this enhancement, the interaction of 4−6 nm Al/$Al_2O_3$ core−shell nanoparticles with a carbon fiber surface at 1000−2500 K is investigated by reactive molecular dynamics. The results show that regardless of the temperature, Al nanoparticles adhere to the surface of the carbon fiber upon interception. At 1000 K, Al nanoparticles adhere through physisorption; however, with increasing temperature, a transition to chemical bonding occurs, marked by the formation of Al−C bonds and the enhanced binding energy between the particle and the surface. The binding energy at 2500 K is 2 orders of magnitude higher than that at 1000 K. Larger Al particles are found to have a stronger binding energy at the same temperature. The sintering of two Al nanoparticles on the surface of the carbon fiber is also examined. Al nanoparticles that are bound to a carbon fiber surface have much lower sintering rates (i.e., the particle shrinkage ratio can be decreased by up to ∼90%, and the particle surface loss ratio can be decreased by up to ∼50%). The discrepancy becomes notably more pronounced at elevated temperatures, where the sintering of Al nanoparticles in the aerosol phase is very fast. The effect of CF addition is to trap burning particles close to the burning surface for a longer time, thereby enhancing heat feedback. This simulation work provides an atomistic-level explanation for our previous experimental works (*ACS Appl. Mater. Interfaces* **2021**, *13*, 30504−30511 and *Chem. Eng. J.* **2023**, *460*, 141653).

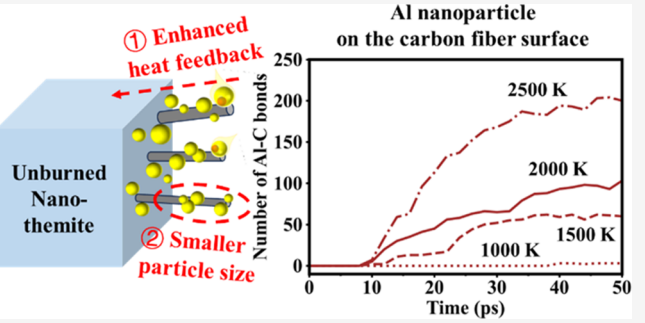




## 1. INTRODUCTION

Aluminum (Al) particles are a common ingredient in explosives, propellants, and pyrotechnics for their high energy density.[1−5] Due to the higher specific surface area of nano vs micron particles, Al nanoparticles usually show a lower ignition temperature and a higher burn rate.[6−8] However, Al nanoparticles also suffer from rapid sintering during or just prior to combustion, which results in a significant particle size increase, which degrades the kinetics and can result in significant two-phase flow losses.[9−11]

One approach to potentially mitigate some of the sintering effects is to decrease the characteristic time for other processes to approach the time scale for sintering or alternatively slow sintering down somehow. The addition of various carbonaceous materials has been shown to be a promising strategy for enhancing the application of Al nanoparticles as well as Al microparticles. Different types of carbonaceous material addition have been studied to modify the ignition and combustion characteristics of Al-based energetic materials, such as carbon fibers,[12,13] hollow carbon nanospheres,[14] carbon black nanoparticles,[15] graphene oxides,[16,17] and carbon nanotubes.[18,19] For instance, Yang et al.[14] examined the influences of hollow carbon nanosphere addition on Al/$Fe_2O_3$ nanothermite and found that hollow carbon nanosphere addition could increase both the burn rate and steady combustion temperature, which they attributed to the gas-generating characteristics of hollow carbon nanospheres. The laser ignition threshold was also lowered due to the good laser adsorption ability of carbon. Jiang et al.[17] studied the addition of graphene oxides in microsized Al particles and found that the graphene oxides can enhance the combustion of Al particles because graphene oxides catalyze the dissociation of oxygen molecules and enhance the diffusion of free oxygen atoms to Al. Sharma et al.[18] reported that the activation energy of the thermite reaction of Al/CuO was lowered by ∼23% by the addition of cabon nanotubes based on its thermogravimetric analysis results. The tighter contacts between Al and

Received: February 23, 2024
Revised: March 25, 2024
Accepted: April 19, 2024
Published: April 30, 2024

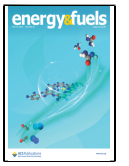




https://doi.org/10.1021/acs.energyfuels.4c00832
*Energy Fuels* 2024, 38, 8992−9000

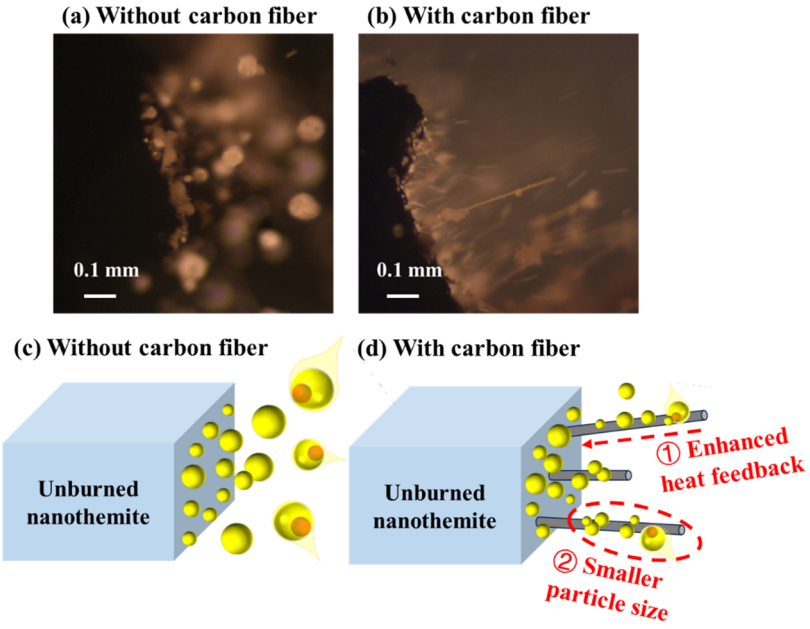


**Figure 1.** Representative microscopic images of the burning Al/CuO nanothermite without (a) and with (b) carbon fibers and the corresponding schematic diagram of the reaction fronts without (c) and with (d) carbon fibers.

CuO due to the presence of carbon nanotubes were concluded as the main reason for such a decrease.

One approach that led to significant effects was the addition of small amounts of carbon fibers.[12,13] Wang et al.[12] found that only 2.5 wt % carbon fiber addition into the Al/CuO nanothermite could increase the global burn rate of the nanothermite by a factor of 2, and the flame temperature was also increased by roughly 300 K. A similar behavior was also reported in our previous research on an Al/AP/HTPB solid propellant.[13] The burn rate of the propellant was elevated by ∼25% after the doping of 2.5 wt % carbon fiber. Figure 1 shows the representative microscopic images of the burning of the Al/CuO nanothermite with and without carbon fiber addition as well as the schematic diagrams on how carbon fibers affect the reaction fronts. The detailed description on experimental methods can be found in our previous study.[12] Although Al particles are initially nanosized, they undergo a transition to microsized particles near the reaction front, owing to rapid sintering. Nevertheless, it is clear that after doping with carbon fibers, the sizes of Al particles are smaller and some of them were intercepted by the carbon fibers that protrude from the reaction front. Correspondingly, two explanations can be proposed for the enhancement caused by the carbon fiber addition. First is that since the Al particles are intercepted by the carbon fibers, they could provide stronger heat feedback to the unburned zone than the free-flowing particles. Second is that the presence of carbon fibers retard Al particle sintering, thus increasing their oxidation rate.

In this work, we employ reactive molecular dynamics (MD) simulations to provide atomic insights into the interaction between Al nanoparticles and the surface of carbon fibers. Both the sticking behavior of Al nanoparticles on carbon fibers and the sintering process of Al nanoparticles with/without carbon fibers are investigated in detail to verify the two explanations in our previous studies as introduced above.

## 2. MD METHODOLOGY

**2.1. Reactive Force Field.** Reactive force field (ReaxFF), developed by van Duin and his coworkers,[20] is employed in this work. ReaxFF offers a more realistic simulation of covalent bond formation and breaking while still being computationally tractable.[21−28] The potential energy $E_p$ of ReaxFF can be described by eq 1.

$$E_p = E_{bond} + E_{over} + E_{under} + E_{lp} + E_{val} + E_{tors} + E_{vdW} + E_{coul} \quad (1)$$

in which the first six items are bond-order-dependent energy items: bond energy, overcoordination energy, under-coordination energy, long pair energy, valence angle energy, and torsion angle energy, respectively; the last two items are bond-order-independent items: van der Waals energy and Coulomb energy, respectively.[20]

The Al/C/H/O force field used in this study was taken from Hong et al.,[29] which was optimized against quantum mechanics data as well as experimental data,[29] and has been employed by others for the simulation of Al nanoparticles in many scenarios similar to this work, such as the carbon coating on Al nanoparticles,[29] the combustion of Al nanoaggregates in high-speed flows,[10] the interaction between graphene oxides and Al nanoparticles,[17] and the combustion of Al/n-butanol nanofluid.[30]

**2.2. Simulation Details.** Al nanoparticles with oxide shells are built in this work by cutting Al and $Al_2O_3$ spheres from ideal aluminum and $\alpha$-alumina lattices, respectively, and annealing. Then, an Al core and an $Al_2O_3$ shell are cut from the annealed spheres and combined into an Al-core−$Al_2O_3$-shell nanoparticle. A few aluminum or oxygen atoms are randomly removed during the construction to make sure the molar ratio of aluminum to oxygen in the oxide shell is nearly 2:3 (0.688, 0.691, and 0.668 for the three particles built in the next paragraph). Then, the Al-core−$Al_2O_3$-shell nanoparticle is relaxed to 400 K.



https://doi.org/10.1021/acs.energyfuels.4c00832
Energy Fuels 2024, 38, 8992−9000

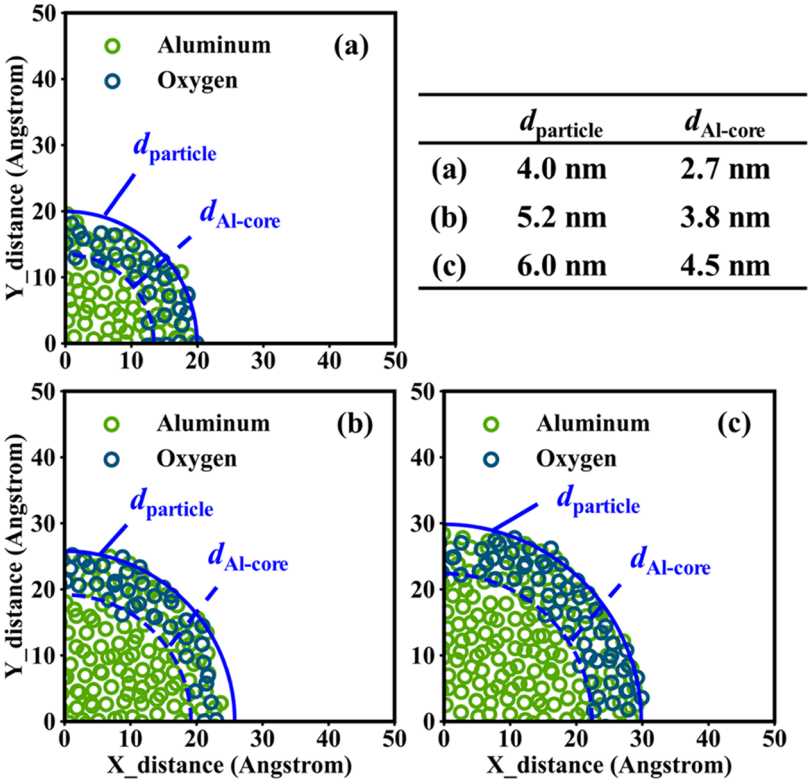


| | $d_{particle}$ | $d_{Al\text{-}core}$ |
|---|---|---|
| (a) | 4.0 nm | 2.7 nm |
| (b) | 5.2 nm | 3.8 nm |
| (c) | 6.0 nm | 4.5 nm |

**Figure 2.** Slices were obtained from Al nanoparticles with different particle diameters. The locations of Al and O atoms are shown in green and dark blue symbols, respectively. The diameters of the particle and the Al core are shown in blue solid and dashed lines, respectively.

Three $Al/Al_2O_3$ core−shell nanoparticles are built, with similar internal structures and thicknesses of the oxide shell but with different particle sizes. In order to show the core−shell structure concisely, slices are cut from the relaxed particles with a thickness of 4 Å, and the positions of all atoms in the slice are shown in Figure 2. The thickness of the slice is in the $z$ direction, and the positions of atoms are projected onto the $X-Y$ plane. The diameters of the entire particle and the Al core are also shown in Figure 2. The diameter of a particle is calculated as the diameter of the smallest sphere that can contain 95% of all atoms. The diameter of the Al core is calculated as the diameter of the largest sphere that can contain only 5% oxygen atoms. The oxide shell thickness of the three particles is ∼0.7 nm. The diameters of three particles are 4.0, 5.2, and 6.0 nm, respectively. For simplicity, they are named 4, 5, and 6 nm Al nanoparticles hereafter. The numbers of atoms in these three particles are 2759, 5629, and 8838, respectively. 2759:5629:8838 is very close to $4^3:5^3:6^3$ because the particle shape is very close to a sphere.

To simulate the carbon fiber, a total of four layers of graphene is employed, following previous studies.[31,32] Similar to the construction of Al nanoparticles, four layers of graphene are cut from ideal graphite, ensuring the sizes of layers align with those of the simulation box. Then, the graphene layers are annealed and relaxed to 400 K, with the layer at the bottom being frozen to maintain surface stability.[23,33−35]

To simulate the binary collision between an Al nanoparticle and the surface of the carbon fiber, a simulation box with a size of 100 × 100 × 150 Å is used. The four layers of graphene, used as the analogue of the carbon fiber surface, are placed at the bottom of the simulation box. Periodic boundary conditions are applied in $x$, $y$, and $z$ directions. The Al nanoparticle is placed above the carbon fiber surface with a separation distance of roughly 0.8 nm. The initial downward velocity of the Al nanoparticle is 15 m/s. The initial velocity setting does not have a significant influence on the conclusions, as explained by Figure S1 in the Supporting Information. The simulation is conducted in the NVT ensemble using a Nose−Hoover thermostat[36] with a damping parameter set as 100 times the time step. The total simulation time is 50 ps, including a 10 ps ramp stage that elevates the temperature from 400 K to 1000/1500/2000/2500 K and a 40 ps constant-temperature stage that is fixed at 1000/1500/2000/2500 K. The temperature fluctuation is negligible, and a representative temperature profile during the simulation is given in the Supporting Information.

To simulate the coagulation and sintering of two Al nanoparticles on the surface of carbon fiber, a simulation box with a size of 120 × 100 × 150 Å is created. The separation distance of the two particles is roughly 1 nm, and the other configuration settings are the same as the binary collision simulations. Each Al nanoparticle has an initial downward velocity of 10 m/s and an initial horizontal velocity of 10 m/s toward the other particle. The simulation without carbon fiber is conducted in the same manner, except that the carbon fiber surface at the bottom of the box and the initial downward velocity of the particle are omitted. The simulation is also conducted in an NVT ensemble, and the total simulation time is 30 ps, including a 10 ps ramp stage and a 20 ps constant-temperature stage, utilizing identical settings to the binary collision simulation introduced in the previous paragraph.

All MD simulations in this work are performed in large-scale atomic/molecular massively parallel simulator (LAMMPS).[37] The time step for all cases is 0.2 fs. The calculation of particle surface area in Section 3.2 is performed in OVITO software.[38]


https://doi.org/10.1021/acs.energyfuels.4c00832
Energy Fuels 2024, 38, 8992−9000

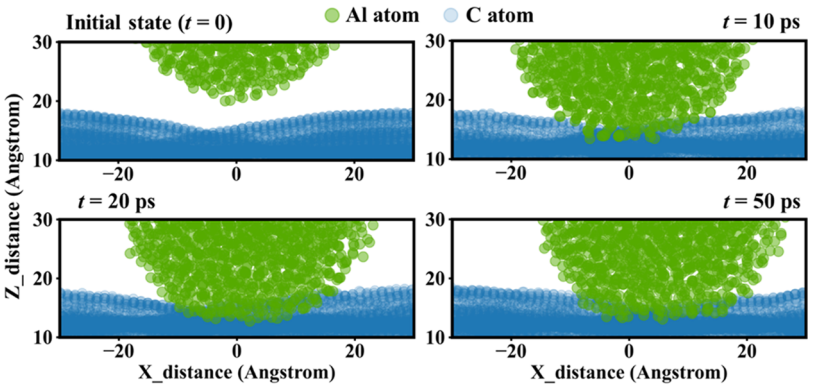


**Figure 3.** Snapshots of the collision between a 4 nm Al nanoparticle and the surface of the carbon fiber at 2000 K. Aluminum atoms are shown in green, and carbon atoms are shown in blue. For simplicity, oxygen atoms are not shown.

## 3. RESULTS AND DISCUSSION

**3.1. Sticking of Al Nanoparticles on the Surface of Carbon Fibers.** In our experiment (Figure 1), Al particles are ejected from a burning surface and are seen to impact carbon fibers, where they stay for an extended period of time and burn (>10 ms). A similar process is simulated. Figure 3 shows snapshots of a typical case, the binary collision between a 4 nm Al nanoparticle and the surface of the carbon fiber at 2000 K. Graphene layers at the bottom of the simulation box are somewhat wave-like due to the thermal expansion. Initially, the Al nanoparticle is far from the carbon fiber surface such that the interaction energy can be neglected. Upon collision, the particle is captured and the particle interacting surface flattens. The position of the captured particle on carbon fiber surface remains nearly constant from $t$ = 20 ps to $t$ = 50 ps, suggesting a stable sticking state, which aligns with experimental observations.[12,13]

To make a detailed analysis of the collision process, we first compare the binary collision results at different temperatures (1000−2500 K), for 4 nm Al nanoparticle. Figure 4(a) presents the evolution of the location of the center of mass (COM) of the Al nanoparticle (the distance between the COM and the bottom of the simulation box) and the interaction energy between the particle and the surface. The location of COM of the Al nanoparticle decreases as the particle approaches the surface and is almost steady after 30 ps. The steady-state locations of the COMs of four simulations at different temperatures are very similar (3.3 nm away from the bottom of the simulation box) and very close to the sum of the radius of the Al nanoparticle (roughly 2 nm) and the thickness of the carbon fiber surface (roughly 1.1 nm), neglecting thermal expansion. It indicates that the Al nanoparticle does not sink into the carbon fiber surface, which is shown in Figure 3 as well. The interaction energy is calculated by eq 2

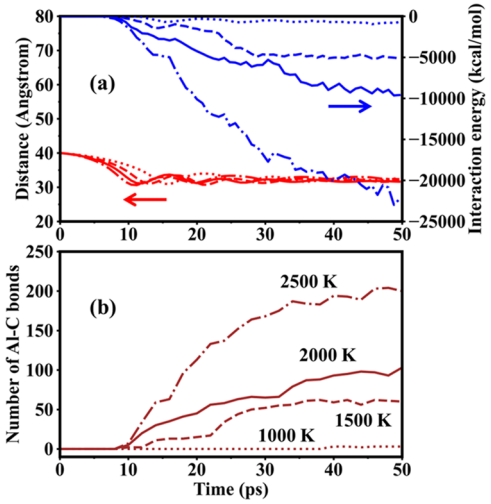


**Figure 4.** (a) Temporal evolution of the distance between the COM of the Al nanoparticle and the bottom of the simulation box (red) and the interaction energy between the Al nanoparticle and the carbon fiber surface (blue) at different temperatures. (b) Temporal evolution of the number of Al−C bonds (brown) at different temperatures. Dotted, dashed, solid, and dashdot lines represent the results at 1000, 1500, 2000, and 2500 K, respectively.

$$E_{\text{interaction}} = E_{\text{p,total}} - E_{\text{p,particle}} - E_{\text{p,surface}} \quad (2)$$

in which $E_{\text{interaction}}$, the interaction energy, can be obtained from the total potential energy of the particle and surface $E_{\text{p,total}}$, the potential energy of particle $E_{\text{p,particle}}$, and the potential energy of surface $E_{\text{p,surface}}$. The interaction energy values are negative, as shown in Figure 4(a), indicating that Al nanoparticles are bound on the carbon fiber surface; thus, the interaction energy will be referred to as the binding energy hereafter.

The results indicate that within a wide range (1000−2500 K), all Al nanoparticles ejected from a combusting surface, if impacted, would be captured by the carbon fiber surface (i.e., no rebound) no matter what the temperature is, which aligns with the experimental observation in Figure 1. When the temperature is low (1000 K), the Al nanoparticle is physisorbed on the carbon fiber, as there is no evidence of the formation of a significant amount of Al−C covalent bonds, as shown in Figure 4(b). The binding energy (Figure 4(a)) is asymptotic to a constant value (∼ −700 kcal/mol) after ∼25 ps, when the Al nanoparticle is stable on the surface. Using the Hamaker constant of alumina from ref 39. ($A_{\text{alumina}}$ = ∼1.5 × $10^{-19}$ J) and graphene from ref 40. ($A_{\text{graphene}}$ = ∼4.7 × $10^{-19}$ J), the interaction Hamaker constant $A$ can be calculated by eq 3[41] to evaluate an empirical estimate for the binding energy from eq 4.

$$A = \sqrt{A_{\text{alumina}} A_{\text{graphene}}} = 2.6 \times 10^{-19}\text{J} \quad (3)$$

$$E_{\text{int,hamaker}} = -\frac{Ad}{12z} N_{\text{A}} = \sim -31\text{kcal/mol} \quad (4)$$



https://doi.org/10.1021/acs.energyfuels.4c00832
Energy Fuels 2024, 38, 8992−9000

where $d$ and $z$ are the diameter of the particle and the separation distance between the particle and the surface, respectively, and $N_A$ is the Avogadro constant. The $z$ value (0.4 nm) is taken from ref 42, representing the typical separation distance for a smooth surface. Compared to the rigid model proposed by Hamaker,[43] it is unsurprising that the binding energy calculated by ReaxFF is higher by an order of magnitude. This discrepancy can largely be attributed to the capability of reactive MD to simulate the deformation of both the Al nanoparticle and the carbon fiber surface, allowing the reconstruction of a more stable configuration, a phenomenon also documented in ref 25. Although there is no chemical bond formation, the physical binding energy is strong enough to capture the ejected Al nanoparticle and prevent rebound.

When the temperature is increased to 1500 K, Al−C bonds form, and the binding energy between Al nanoparticles and the carbon fiber is enhanced significantly. Further increasing temperature results in more Al−C bonds and correspondingly stronger binding energy, making the Al nanoparticle firmly anchored onto the carbon fiber surface. At 2500 K, the binding energy between the particle and the surface is already more than 20 000 kcal/mol, as shown in Figure 4(a), not only preventing the dissociation but also inhibiting the movement of the particle on the surface, the significance of which will be discussed in Section 3.2.

The influence of the particle size on the sticking is also investigated, as illustrated in Figure 5. The simulation

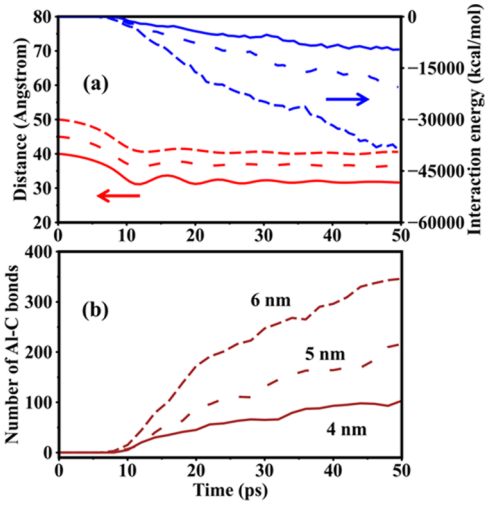


**Figure 5.** (a) Temporal evolution of the distance between the COM of the Al nanoparticle and the bottom of the simulation box (red) and the interaction energy between the Al nanoparticle and the carbon fiber surface (blue) for different particle sizes. (b) Temporal evolution of the number of Al−C bonds (brown) for different particle sizes. Solid, loosely dashed, and densely dashed lines represent the results for 4, 5, and 6 nm particles, respectively.

temperature, corresponding roughly to the flame temperature, is 2000 K. As expected, the steady-state locations of COMs of three Al nanoparticles are different since their diameters are different. We can also note that the binding energy increases with particle size. As depicted in Figure 3, Al nanoparticles exhibit slight deformation. Larger particles would have a bigger contact area with the carbon fiber surface, providing more sites for the formation of Al−C bonds to enhance the binding energy.

**3.2. Coagulation and the Sintering Process of Al Nanoparticles on the Surface of Carbon Fibers.** As discussed in the introduction, sintering is a significant process in nanoparticles and is thought to retard burning kinetics.[44] Figure 6 illustrates snapshots (projected onto the $X$−$Z$ plane) of two Al nanoparticles and a carbon fiber surface at 1000 K. At such a low temperature, the two Al nanoparticles are only slightly sintered after coagulation due to the presence of the solid $Al_2O_3$ shell. On the other hand, particles physisorbed onto the carbon fiber show lower mobility and slower sintering kinetics. To quantitively describe the degree of sintering, we examine the evolution of the dimensionless distance $d/d_0$ and the dimensionless surface area $S/S_0$, where $d$ and $S$ are the real-time distance between the COMs and the real-time surface area of the two Al nanoparticles. $d_0$ and $S_0$ are initial values of the particle diameter and the particle surface area. In order to make a comparison, the distance $d_{\text{unsintered}}$ and surface $S_{\text{unsintered}}$, assuming no sintering, are also calculated by eq 5 and 6. Thermal expansion is taken into account as

$$\frac{d_{\text{unsintered}}}{d_0} = 1 + \alpha\Delta T \tag{5}$$

$$\frac{S_{\text{unsintered}}}{S_0} = (1 + \alpha\Delta T)^2 \tag{6}$$

in which $\alpha$ is the linear thermal expansion coefficient of the $Al_2O_3$ shell and $\Delta T$ is the temperature difference (K). The $\alpha$ value ($12.66 \times 10^{-6}$ $K^{-1}$) is taken from ref 45. Thermal expansion of the particle surface before sintering can be well predicted by $\alpha$, as depicted in the overlapping calculated and simulated surface evolution profiles during the ramping stage in Figures 7 and 9.

Figure 7 depicts the evolution of $d/d_0$, $S/S_0$, $d_{\text{unsintered}}/d_0$, and $S_{\text{unsintered}}/S_0$ of two Al nanoparticles at 1000 K. In the free coagulation (aerosol) simulation, two particles collide with each other at ∼8 ps (the intersection of $d/d_0$-curve and $d_{\text{unsintered}}/d_0$-curve). After the collision, two particles move closer and lead to a decrease in $d/d_0$ and $S/S_0$. In the simulation with the carbon fiber, they collide at ∼15 ps; i.e., later than the free coagulation case. However, for both cases, $d/d_0$ and $S/S_0$ are almost unchanged after 20 ps, forming a "flat stage". Since the temperature is not very high, the sintering is not significant. The contours of the two particles remain distinctly observable, as shown in Figure 6. The sintered particle surface area is still nearly 90% of the unsintered particle surface area.

Figure 8 illustrates what occurs at 2000 K. Unlike the simulation at 1000 K, sintering is much more significant for the particles in the aerosol phase (left part of Figure 8), as sintering kinetics of nanoparticles is highly dependent on temperature.[46] The outlines of the two Al nanoparticles become indistinct and blurred. In contrast, particles on fibers show significantly less sintering. This is because the formation of Al−C bonds at this temperature appears to significantly retard the ability of the dimerized particle to move.

Figure 9 shows the evolution of $d/d_0$, $S/S_0$, $d_{\text{unsintered}}/d_0$, and $S_{\text{unsintered}}/S_0$ for two Al nanoparticles at 2000 K. It can be found that the inhibition on particle sintering by the carbon fiber surface is very obvious at such a high temperature. With the carbon fiber, the surface area loss is decreased by a factor of ∼2. It can also be noted that $d/d_0$ has a slight decreasing tendency even at the "flat stage" for free coagulation


https://doi.org/10.1021/acs.energyfuels.4c00832
Energy Fuels 2024, 38, 8992−9000

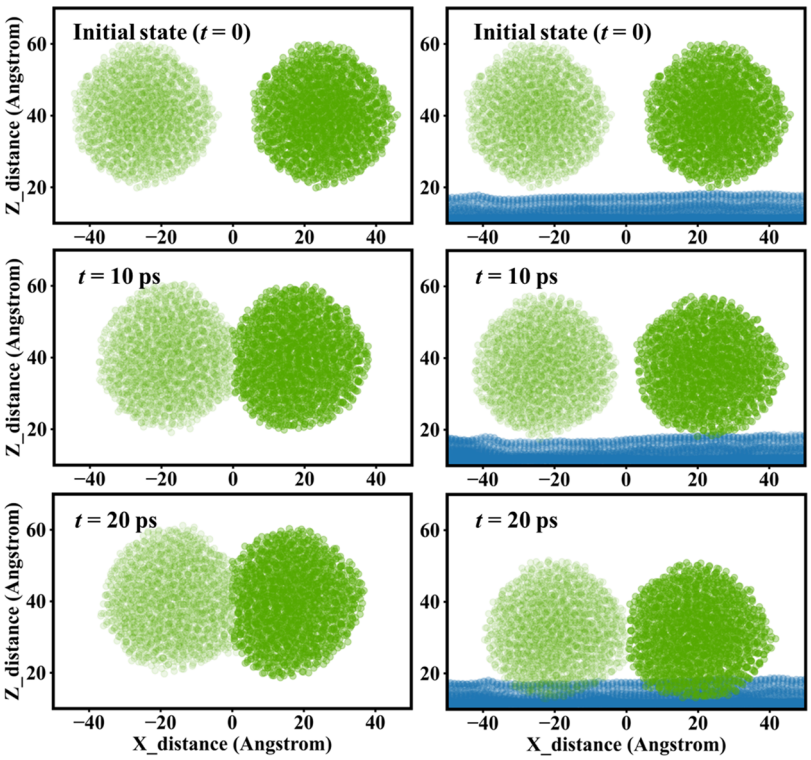


**Figure 6.** Snapshots of two 4 nm Al nanoparticles in the aerosol phase and on a carbon fiber surface undergoing coagulation and/or sintering at 1000 K. Carbon atoms are shown in blue. Aluminum atoms from two different particles are distinguished by dark and light green. For simplicity, oxygen atoms are not shown.

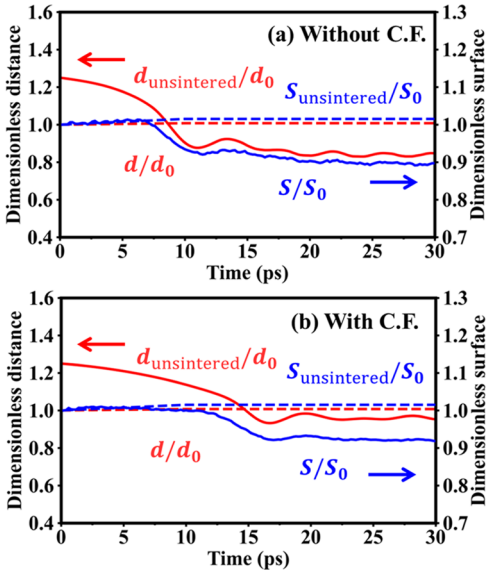


**Figure 7.** Temporal evolution of $d/d_0$ (red solid line), $S/S_0$ (blue solid line), $d_{unsintered}/d_0$ (red dashed line), and $S_{unsintered}/S_0$ (blue dashed line) for two 4 nm Al nanoparticles during their coagulation at 1000 K with (a) and without (b) the carbon fiber.

simulation, which cannot be observed at 1000 K and can be attributed to the thermal driven diffusion of Al atoms inside the sintered particles, as shown in Figures 6 and 8.

Temporal evolution of $d/d_0$, $S/S_0$, $d_{unsintered}/d_0$, and $S_{unsintered}/S_0$ during the coagulation and sintering processes at 1500 and 2500 K can be found in the Supporting Information.

In summary, the interception of aluminum particles by a carbon fiber significantly inhibits sintering, particularly at higher temperatures where the sintering in the aerosol phase is very severe. To quantitatively show this tendency, the shrinkage ratio and the surface loss ratio for two Al nanoparticles at 1000, 1500, 2000, and 2500 K with and without the carbon fiber are estimated based on eqs 7 and 8, and the results are presented in Figure 10.

$$\text{Shrinkageratio} = \frac{d_{\text{unsintered,final}} - d_{\text{final}}}{d_{\text{unsintered,final}}} \quad (7)$$

$$\text{Surfacelossratio} = \frac{S_{\text{unsintered,final}} - S_{\text{final}}}{S_{\text{unsintered,final}}} \quad (8)$$

in which $d_{final}$, $d_{unsintered,\ final}$, $S_{final}$, and $S_{unsintered,\ final}$ are the respective values of $d$, $d_{unsintered}$, $S$, and $S_{unsintered}$ at the end of simulation, where they are already steady and can hardly further change with time.

In general, higher temperatures promote Al nanoparticle sintering; however, the particles residing on a carbon fiber show a much slower sintering rate. This tendency is also supported by the microscopic images of the reaction fronts of Al/CuO nanothermite doping with the carbon fiber (Figure 1), and it should be clear that reduced sintering would be very beneficial to the oxidation of Al nanoparticles, leading to enhanced flame propagation.[12]

## 4. CONCLUSIONS

Previous experimental observations have shown that the addition of the carbon fiber can significantly promote the propagation of the aluminum-based nanothermite and the propellant. In the present work, the reasons for the enhancement of carbon fiber addition on the propagation of aluminum-based nanoenergetics are explored at the molecular


https://doi.org/10.1021/acs.energyfuels.4c00832
Energy Fuels 2024, 38, 8992−9000

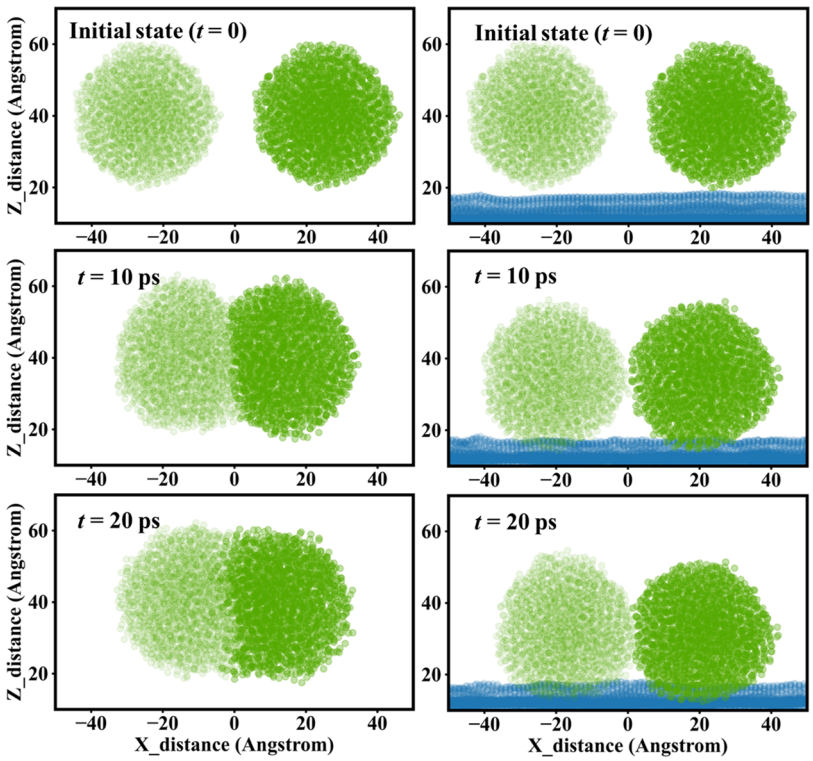


**Figure 8.** Snapshots of two 4 nm Al nanoparticles in the aerosol phase and on a carbon fiber surface, undergoing coagulation and/or sintering at 2000 K. Carbon atoms are shown in blue. Aluminum atoms from two different particles are distinguished by dark and light green. For simplicity, oxygen atoms are not shown.

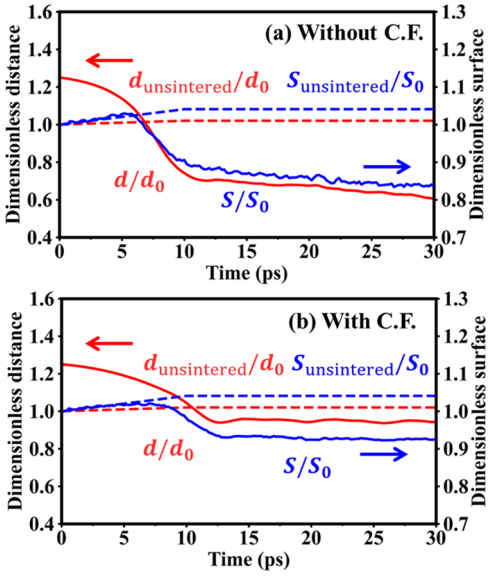


**Figure 9.** Temporal evolution of $d/d_0$ (red solid line), $S/S_0$ (blue solid line), $d_{unsintered}/d_0$ (red dashed line), and $S_{unsintered}/S_0$ (blue dashed line) of two 4 nm Al nanoparticles during their coagulation at 2000 K with (a) and without (b) the carbon fiber.

level. Reactive molecular dynamics simulation is employed to study the interaction between an Al nanoparticle (that would be emanated from a burning solid composite) and the surface of the carbon fiber used as a dopant. The $Al/Al_2O_3$ core–shell nanoparticle used in this work varies from 4 to 6 nm, and the temperature varies from 1000 to 2500 K. The main conclusions can be summarized as

(1) The collision between the Al nanoparticle and the carbon fiber surface results in the sticking of the particle to the surface. No rebound is observed, which is consistent with the experimental imaging results. When the temperature is low (1000 K), the Al nanoparticle is physisorbed to the carbon fiber. Increasing temperature shows a transition to chemical adsorption between the particle and the carbon surface via the formation of Al–C bonds, which significantly increases the binding energy between the Al nanoparticle and the carbon fiber surface, allowing the Al nanoparticle to have a stable residence near the reaction front.

(2) Larger particles have larger binding energy due to the larger contact area with the surface and consequent more Al–C bonds.

(3) Sintering between two Al nanoparticles is very temperature sensitive: accelerating at higher temperatures. However, particles attached to the carbon fiber have much lower sintering rates as the strong binding between the particle and the surface restricts the movement of particles. The shrinkage ratio of two Al nanoparticles decreases from ~0.56 to ~0.05 with the carbon fiber, and the surface loss ratio decreases from ~0.2 to ~0.1 at 2500 K.

The capture of particles by the carbon fiber extends the residence time of particles near the reaction front and therefore enhances heat feedback to the unburned zone. The inhibition of particle sintering reduces surface loss and, therefore, promotes Al nanoparticle oxidation. These microscopic results are in qualitative agreement with our previous experimental observations and provide a molecular basis for our previous explanations.


https://doi.org/10.1021/acs.energyfuels.4c00832
Energy Fuels 2024, 38, 8992–9000

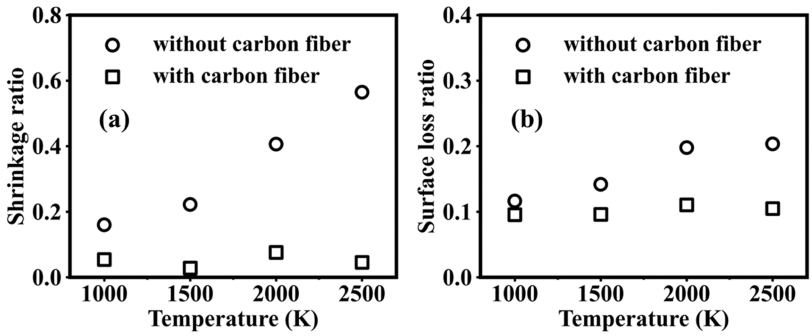


**Figure 10.** Shrinkage ratio (a) and surface loss ratio (b) of two 4 nm Al nanoparticles with and without the surface of the carbon fiber.

## ■ ASSOCIATED CONTENT

### Supporting Information

The Supporting Information is available free of charge at https://pubs.acs.org/doi/10.1021/acs.energyfuels.4c00832.

A typical temporal evolution of the temperature of the binary collision simulation between a 4 nm Al nanoparticle and the carbon fiber surface; temporal evolution of the distance between the COM of the Al nanoparticle and the bottom of the simulation box and the interaction energy between the Al nanoparticle and the carbon fiber surface for different initial velocities and angles of incidence; temporal evolution of the number of Al−C bonds for different initial velocities and angles of incidence; and temporal evolution of $d/d_0$, $S/S_0$, $d_{\text{unsintered}}/d_0$, and $S_{\text{unsintered}}/S_0$ of two 4 nm Al nanoparticles during their coagulation at 1500/2500 K with/without the carbon fiber (PDF)

## ■ AUTHOR INFORMATION


### Corresponding Author

**Michael R. Zachariah** − *Department of Chemical and Environmental Engineering, University of California, Riverside, California 92521, United States;* orcid.org/0000-0002-4115-3324; Email: mrz@engr.ucr.edu

### Author

**Yuxin Zhou** − *Department of Chemical and Environmental Engineering, University of California, Riverside, California 92521, United States;* orcid.org/0009-0005-1397-3834

Complete contact information is available at: https://pubs.acs.org/10.1021/acs.energyfuels.4c00832


### Notes

The authors declare no competing financial interest.

## ■ ACKNOWLEDGMENTS

This research has been supported by the US Army Collaborative Center for Energetic Materials Basic Research and the Office of Naval Research.

## ■ REFERENCES


(1) Ma, X.; Li, Y.; Hussain, I.; Shen, R.; Yang, G.; Zhang, K. Core−shell structured nanoenergetic materials: preparation and fundamental properties. *Adv. Mater.* **2020**, *32*, No. 2001291.

(2) Dreizin, E. L. Metal-based reactive nanomaterials. *Prog. Energy Combust. Sci.* **2009**, *35* (2), 141−167.

(3) Pang, W.; Li, Y.; DeLuca, L. T.; Liang, D.; Qin, Z.; Liu, X.; et al. Effect of metal nanopowders on the performance of solid rocket propellants: A review. *Nanomaterials* **2021**, *11* (10), 2749.

(4) Patel, V. K.; Joshi, A.; Kumar, S.; Rathaur, A. S.; Katiyar, J. K. Molecular combustion properties of nanoscale aluminum and its energetic composites: a short review. *ACS Omega* **2021**, *6* (1), 17−27.

(5) Yetter, R. A. Progress towards nanoengineered energetic materials. *Prog. Energy Combust. Sci.* **2021**, *38* (1), 57−81.

(6) Sundaram, D. S.; Yang, V.; Zarko, V. E. Combustion of nano aluminum particles. *Combust., Explos. Shock Waves* **2015**, *51*, 173−196.

(7) Sundaram, D. S.; Puri, P.; Yang, V. A general theory of ignition and combustion of nano-and micron-sized aluminum particles. *Combust. Flame* **2016**, *169*, 94−109.

(8) Wang, J.; Qu, Y.; Gong, F.; Shen, J.; Zhang, L. A promising strategy to obtain high energy output and combustion properties by self-activation of nano-Al. *Combust. Flame* **2019**, *204*, 220−226.

(9) Galfetti, L.; DeLuca, L.; Severini, F.; Colombo, G.; Meda, L.; Marra, G. Pre and post-burning analysis of nano-aluminized solid rocket propellants. *Aerosp. Sci. Technol.* **2007**, *11* (1), 26−32.

(10) Chu, Q.; Chang, X.; Chen, D. A physiochemical model for the combustion of aluminum nano-agglomerates in high-speed flows. *Combust. Flame* **2022**, *237*, No. 111739.

(11) Wang, H.; Kline, D. J.; Biswas, P.; Zachariah, M. Connecting agglomeration and burn rate in a thermite reaction: Role of oxidizer morphology. *Combust. Flame* **2021**, *231*, No. 111492.

(12) Wang, H.; Kline, D. J.; Rehwoldt, M. C.; Zachariah, M. Carbon fibers enhance the propagation of high loading nanothermites: In situ observation of microscopic combustion. *ACS Appl. Mater. Interfaces* **2021**, *13* (26), 30504−30511.

(13) Wang, H.; Hagen, E.; Shi, K.; Herrera, S.; Xu, F.; Zachariah, M. Carbon fibers as additives to engineer agglomeration and propagation of aluminized propellants. *Chem. Eng. J.* **2023**, *460*, No. 141653.

(14) Yang, H.; Xu, C.; Man, S.; Bao, H.; Xie, Y.; Li, X.; et al. Effects of hollow carbon nanospheres on combustion performance of Al/Fe2O3-based nanothermite sticks. *J. Alloys Compd.* **2022**, *918*, No. 165684.

(15) Bach, A.; Gibot, P.; Vidal, L.; Gadiou, R.; Spitzer, D. Modulation of the reactivity of a WO3/Al energetic material with graphitized carbon black as additive. *J. Energy Mater.* **2015**, *33* (4), 260−276.

(16) Su, J.; Hu, Y.; Zhou, B.; Ye, Y.; Shen, R. The Role of Graphene Oxide in the Exothermic Mechanism of Al/CuO Nanocomposites. *Molecules* **2022**, *27* (21), 7614.

(17) Jiang, Y.; Deng, S.; Hong, S.; Zhao, J.; Huang, S.; Wu, C.-C.; et al. Energetic performance of optically activated aluminum/graphene oxide composites. *ACS Nano* **2018**, *12* (11), 11366−11375.

(18) Sharma, M.; Sharma, V. Effect of carbon nanotube addition on the thermite reaction in the Al/CuO energetic nanocomposite. *Philos. Mag.* **2017**, *97* (22), 1921−1938.

(19) Kim, J. H.; Cho, M. H.; Kim, K. J.; Kim, S. H. Laser ignition and controlled explosion of nanoenergetic materials: The role of multi-walled carbon nanotubes. *Carbon* **2017**, *118*, 268−277.

(20) Van Duin, A. C. T.; Dasgupta, S.; Lorant, F.; Goddard, W. A. ReaxFF: a reactive force field for hydrocarbons. *J. Phys. Chem. A* **2001**, *105* (41), 9396−9409.

(21) Chen, Z.; Sun, W.; Zhao, L. Combustion mechanisms and kinetics of fuel additives: A reaxff molecular simulation. *Energy Fuels* **2018**, *32* (11), 11852−11863.
(22) Li, X.; Zheng, M.; Ren, C.; Guo, L. ReaxFF molecular dynamics simulations of thermal reactivity of various fuels in pyrolysis and combustion. *Energy Fuels* **2021**, *35* (15), 11707−11739.
(23) Zhou, Y.; Chu, Q.; Hou, D.; Chen, D.; You, X. Molecular dynamics study on the condensation of PAH molecules on quasi soot surfaces. *J. Phys. Chem. A* **2022**, *126* (4), 630−639.
(24) Zhou, Y.; Hou, D.; You, X. Effects of Iron Addition on the Collision of Polycyclic Aromatic Hydrocarbon Clusters: A Molecular Dynamics Study. *J. Phys. Chem. A* **2023**, *127* (4), 1026−1035.
(25) Hou, D.; Pascazio, L.; Martin, J.; Zhou, Y.; Kraft, M.; You, X. On the reactive coagulation of incipient soot nanoparticles. *J. Aerosol Sci.* **2022**, *159*, No. 105866.
(26) Liu, S.; Wei, L.; Zhou, Q.; Yang, T.; Li, S.; Zhou, Q.; et al. Simulation strategies for ReaxFF molecular dynamics in coal pyrolysis applications: A review. *J. Anal. Appl. Pyrolysis* **2023**, *170*, No. 105882.
(27) Xiao, Y.; Zeng, J.-F.; Liu, J.-W.; Lu, X.; Shu, C.-M. Reactive force field (ReaxFF) molecular dynamics investigation of bituminous coal combustion under oxygen-deficient conditions. *Fuel* **2022**, *318*, No. 123583.
(28) Qiu, Y.; Zhong, W.; Yu, A. Simulations on pressurized oxy-coal combustion and gasification by molecular dynamics method with ReaxFF. *Adv. Powder Technol.* **2022**, *33* (5), No. 103557.
(29) Hong, S.; Van Duin, A. C. T. Atomistic-scale analysis of carbon coating and its effect on the oxidation of aluminum nanoparticles by ReaxFF-molecular dynamics simulations. *J. Phys. Chem. C* **2016**, *120* (17), 9464−9474.
(30) Cheng, Y.-X.; Zhao, Y.; Zhao, F.-Q.; Xu, S.-Y.; Ju, X.-H.; Ye, C.-C. ReaxFF simulations on the combustion of Al and n-butanol nanofluid. *Fuel* **2022**, *330*, No. 125465.
(31) Tam, L-h.; Jiang, J.; Yu, Z.; Orr, J.; Wu, C. Molecular dynamics investigation on the interfacial shear creep between carbon fiber and epoxy matrix. *Appl. Surf. Sci.* **2021**, *537*, No. 148013.
(32) Wang, H.; Jin, K.; Wang, C.; Guo, X.; Chen, Z.; Tao, J. Effect of fiber surface functionalization on shear behavior at carbon fiber/epoxy interface through molecular dynamics analysis. *Composites, Part A* **2019**, *126*, No. 105611.
(33) Wang, S.; Zhou, G.; Ma, Y.; Gao, L.; Song, R.; Jiang, G.; Lu, G. Molecular dynamics investigation on the adsorption behaviors of H2O, CO2, CH4 and N2 gases on calcite (1 1 0) surface. *Appl. Surf. Sci.* **2016**, *385*, 616−621.
(34) Cai, S.; Li, Q.; Liu, C.; Zhou, Y. Evaporation of R32/R152a mixtures on the Pt surface: A molecular dynamics study. *Int. J. Refrig.* **2020**, *113*, 156−163.
(35) Chu, Q.; Shi, B.; Wang, H.; Chen, D.; Liao, L. Hydrogen abstraction/addition reactions in soot surface growth. *Phys. Chem. Chem. Phys.* **2021**, *23*, 3071−3086.
(36) Evans, D. J.; Holian, B. L. The nose−hoover thermostat. *J. Phys. Chem. A* **1985**, *83* (8), 4069−4074.
(37) Plimpton, S. Fast parallel algorithms for short-range molecular dynamics. *J. Comput. Phys.* **1995**, *117* (1), 1−19.
(38) Stukowski, A. Visualization and analysis of atomistic simulation data with OVITO−the Open Visualization Tool. *Modell. Simul. Mater. Sci. Eng.* **2010**, *18* (1), No. 015012.
(39) Bergström, L. Hamaker constants of inorganic materials. *Adv. Colloid Interface Sci.* **1997**, *70*, 125−169.
(40) Dahneke, B. The influence of flattening on the adhesion of particles. *J. Colloid Interface Sci.* **1972**, *40* (1), 1−13.
(41) Drauglis, E. *Molecular Processes on Solid Surfaces*. McGraw-Hill, 1969.
(42) Hinds, W. C.; Zhu, Y. *Aerosol technology: properties, behavior, and measurement of airborne particles*; John Wiley & Sons, 2022.
(43) Hamaker, H. C. The London-van der Waals attraction between spherical particles. *Physica* **1937**, *4* (10), 1058−1072.
(44) Chakraborty, P.; Zachariah, M. Do nanoenergetic particles remain nano-sized during combustion? *Combust. Flame* **2014**, *161* (5), 1408−1416.
(45) Balakrishnan, G.; Thirumurugesan, R.; Mohandas, E.; Sastikumar, D.; Kuppusami, P.; Song, J. I. Phase transition and thermal expansion studies of alumina thin films prepared by reactive pulsed laser deposition. *J. Nanosci. Nanotechnol.* **2014**, *14* (10), 7728−7733.
(46) Zachariah, M.; Carrier, M. J. Molecular Dynamics Computation of Nanoparticle Sintering: Comparison with Phenomenological Models. *J. Aerosol Sci.* **1999**, *30* (9), 1139−1151.


https://doi.org/10.1021/acs.energyfuels.4c00832
*Energy Fuels* 2024, 38, 8992−9000